AGU PUBLICATIONS

Geophysical Research Letters

The five stable noble gases are sensitive unambiguous tracers of glacial meltwater

B. Loose[1] and W. J. Jenkins[2]

[1]Graduate School of Oceanography, University of Rhode Island, Narragansett, Rhode Island, USA, [2]Woods Hole Oceanographic Institution, Woods Hole, Massachusetts, USA

Abstract The five inert noble gases—He, Ne, Ar, Kr, and Xe—exhibit a unique dissolved gas saturation pattern resulting from the formation and addition of glacial meltwater to seawater. He and Ne become oversaturated, and Ar, Kr, and Xe become undersaturated to varying percentages. For example, addition of 10‰ glacial meltwater to seawater results in a saturation anomaly of $\Delta He = 12.8\%$, $\Delta Ne = 8.9\%$, $\Delta Ar = -0.5\%$, $\Delta Kr = -2.2\%$, and $\Delta Xe = -3.3\%$. This pattern in noble gas saturation reflects a unique meltwater signature that is distinct from the other major physical processes that modify the gas concentration and saturation, namely, seasonal changes in temperature at the ocean surface and bubble mediated gas exchange. We use Optimum Multiparameter analysis to illustrate how all five noble gases can help distinguish glacial meltwater from wind-driven bubble injection, making them a potentially valuable suite of tracers for glacial melt and its concentration in the deep waters of the world ocean.

1. Introduction

The ice shelf of a marine-terminating glacier is a fundamental support structure that mitigates the flow rate of glacial ice toward the coast and eventual demise through melting and calving [*Jacobs et al.*, 1992]. When floating ice shelves collapse, the upstream glacier flows more quickly into the sea [*Alley et al.*, 2005]. Consequently, we seek to understand and monitor the stability of floating ice shelves. An ice shelf loses mass from surface ablation, calving, and basal melt along its underside, which is in contact with seawater. Estimating the rate of basal melt is the most challenging [*Rignot and Jacobs*, 2002], because it is difficult to observe and it is likely sensitive to changes in ocean temperature [*Holland and Jenkins*, 1999] and other ocean processes such as the sea ice cycle. In addition to affecting glacial mass balance, the ice shelves in the Weddell and Ross Seas influence the composition of the densest water masses of the world ocean [*Schlosser et al.*, 1987; *Orsi et al.*, 1999]. The water masses in both of these marginal seas are freshening [*Jacobs et al.*, 2002; *Hellmer et al.*, 2011] and there is evidence that Antarctic Bottom Water is responding rapidly to changes in surface ocean forcing by becoming warmer [*Jullion et al.*, 2010; *Meredith et al.*, 2011].

The five stable noble gases (NGs) do not participate in the biology and chemistry of the ocean, making them excellent inert tracers for a range of climatically important physical processes in the ocean. For example, He, Ne, Ar, Kr, and their isotopes have been used to estimate the rate of diapycnal mixing in the equatorial thermocline [*Emerson et al.*, 2012], observe the rates and mechanics of deep-water ventilation [*Hamme and Severinghaus*, 2007; *Nicholson et al.*, 2010; *Ito et al.*, 2011], and the rate of air-sea gas exchange, either by diffusion or by bubble subduction [*Hamme and Emerson*, 2006; *Stanley et al.*, 2006]. Helium and neon are also valuable as tracers for glacial meltwater [*Schlosser*, 1986; *Schlosser et al.*, 1990; *Hohmann et al.*, 2002; *Rodehacke et al.*, 2006; *Loose et al.*, 2009]. When glacial ice melts at depth, air that was trapped in the ice matrix dissolves in the water, under pressure, causing He and Ne to exhibit excess saturation. The resulting trace gas composition is unique from seawater, and the concentrations of He and Ne stand out above their backgrounds. However, both glacial melt and high wind bubble injection at the air-sea interface produce a similar excess saturation in He and Ne. Without the aid of additional tracers, there is a potential ambiguity between the contribution of glacial meltwater and bubble-driven gas exchange to the deep pools of the ocean [*Hamme and Severinghaus*, 2007]. This ambiguity can also lead to uncertainty in tracing glacial meltwater, especially far from its ice shelf sources and under extreme dilution.

In this short contribution, our intent is to show that glacial meltwater and bubble injection are distinguishable when using the five stable NGs. The heavier NGs are significantly more soluble in seawater, their solubility is

more sensitive to changes in temperature and salinity, and their atmospheric concentrations are unique from those of He and Ne. These factors combine to produce gas concentrations and saturation anomalies that are distinct from the other physical processes that affect these gases. We illustrate this distinction using an empirical relationship for bulk air bubble injection and the addition of melted glacial ice to seawater. By applying the Optimal Multiparameter (OMP) method to a hypothetical ocean surface with wind-driven air bubble injection and meltwater addition, we attempt to demonstrate the quantitative separation of the two processes.

2. Methods

Changes in the heat and salt content of ambient seawater, wave breaking, freezing and melting of both glacial and marine ice, and synoptic changes in the atmospheric pressure can all affect the dissolved gas content of seawater [*Hamme and Severinghaus*, 2007]. The easiest means to express the effect of these processes on gas content is with the saturation anomaly, Δ, an expression of the observed gas content (C_{obs}) with reference to the gas content to be expected if seawater were in solubility equilibrium with the atmosphere (C_{eq}) $\Delta C \ (\text{in} \%) = \left(\frac{C_{obs}}{C_{eq}} - 1 \right) \times 100$. The saturation anomaly reflects the excess or deficit gas content that a water mass would exhibit if it was transferred adiabatically to the ocean surface. Here we use the Δ notation to compare the effects of heating, cooling, wind-driven bubble injection, and meltwater addition. The Δ values have been calculated using the noble gas solubility functions distributed by Roberta Hamme (http://web.uvic.ca/~rhamme/download.html). The Xe solubility has been additionally decreased by 2% as proposed by *Hamme and Severinghaus* [2007].

2.1. Noble Gases in Sea Surface Air Bubbles

Air trapped beneath breaking waves can result in excess saturation as gas bubbles are forced into solution under increasing hydrostatic pressure [*Keeling*, 1993] and can be an important process in air-sea gas fluxes [*Goddijn-Murphy et al.*, 2012]. To represent the effect of bubble injection on the saturation anomaly, we simulate air bubble injection using the total air bubble injection flux equation (F_{BI}) in mol m^{-2} s^{-1} from *Stanley et al.* [2006], $F_{BI} = 9.1 \times 10^{-11}(U_{10} - 2.27)^3 \frac{P}{RT}$, where U_{10} is the 10 m wind speed, P, R, and T are the pressure, gas constant, and temperature, respectively. When divided by the mixed layer depth (100 m in the case of Figure 1), F_{BI} gives an estimate of the air injection rate in the upper ocean. While this empirical relationship is thought to produce realistic bubble injection results, the choice of bubble entrainment relationship is not central to this analysis as it predicts the bulk amount of air subducted and we are concerned with the differential response of the NGs as opposed to the total quantity of gas bubble injection.

Using this relationship and a constant wind speed of 10 m s^{-1} blowing for 25 days produces an integrated bubble flux of approximately 8.8×10^{-4} cm^3 STP g^{-1} of air and saturation anomalies of ΔHe = 11.6%, ΔNe = 8.8%, ΔAr = 2.1%, ΔKr = 1.1%, and ΔXe = 0.5% in seawater of $S = 34$ and $T = 0$°C. All the NGs are oversaturated, but the effect is diminished for heavier NGs, given their greater solubility in water. The resulting gas ratios are $\frac{\Delta He}{\Delta Ar} = 5.4$, $\frac{\Delta Ne}{\Delta Ar} = 4.1$, $\frac{\Delta Kr}{\Delta Ar} = 0.5$, and $\frac{\Delta Xe}{\Delta Ar} = 0.2$ (Figure 1).

A second bubble injection process known as partial bubble exchange results when larger air bubbles are only partially dissolved before floating back to the surface [*Keeling*, 1993]. The process is similar to diffusive gas exchange as it depends on the air-water gas differential and the molecular diffusivity of each gas. Consequently, excess saturation anomalies from partial bubble exchange are nearly 1:1 for each of the NGs so that this process has a projection that is much closer to seasonal heating-cooling than to meltwater addition (Figure 1). Partial bubble exchange is thought to be less significant in producing excess saturation [*Hamme and Emerson*, 2006; *Stanley et al.*, 2006], with an air contribution of 2:1 bubble injection:partial bubble exchange [*Hamme and Emerson*, 2006; *Stanley et al.*, 2006].

2.2. Noble Gases in Glacial Meltwater

The average air content in glacial ice cores on Antarctica is 0.11 g cm^{-3}, based on samples from 14 drill sites around Antarctica [*Martinierie et al.*, 1992; *Hohmann et al.*, 2002]. This air is trapped during snow deposition and remains trapped as snow evolves to firn and then to ice. Several artifacts are known to alter the noble gas concentration in glacial ice. The first is a slight depletion of neon from differential diffusion through glacial firn [*Severinghaus and Battle*, 2006]; this effect can alter the neon content in glacial meltwater by less than 1%, and it does not affect the larger NGs—Ar, Kr, and Xe. In contrast, the stratification of gases in the firn layer based on
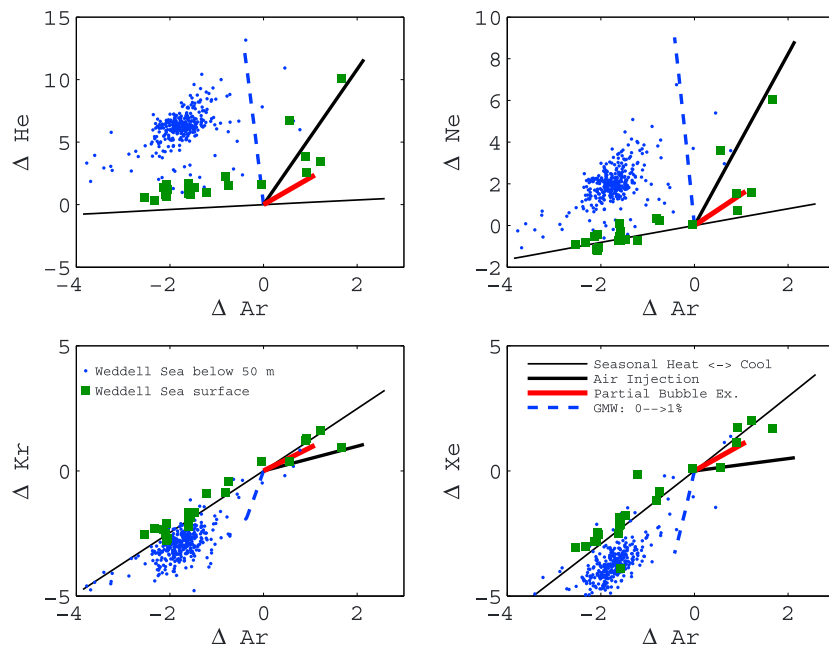
Figure 1. Processes that lead to an excess or deficit noble gas saturation anomaly: seasonal heating and cooling (thin line), air bubble injection (thicker line), partial bubble exchange (thickest line), and addition of glacial meltwater (dashed line). The discrete points are from noble gas samples taken in the Weddell Sea in 2010; filled squares are samples collected in the top 50 m of the water column, and solid circles are all the subsurface samples.

their molecular weight has a slightly larger effect. This process, known as gravitational enrichment, results in an approximately 7% increase in the He/Xe ratio in glacial ice as compared to the atmosphere [*Craig et al.*, 1988]. The effect can be accounted for using the temperature and close-off depth of the firn layer.

As this glacial ice melts at depth, it is posited that the air content is forced into solution [*Schlosser*, 1986; *Hohmann et al.*, 2002; *Loose et al.*, 2009]. A 10‰ addition of glacial meltwater to ambient seawater of $S = 34$ and $T = 0°C$ results in gas saturation anomaly of $\Delta He = 12.8\%$, $\Delta Ne = 8.9\%$, $\Delta Ar = -0.5\%$, $\Delta Kr = -2.2\%$, and $\Delta Xe = -3.3\%$. The analytical precision for the noble gases is 0.5% (0.3% for Kr) [*Stanley et al.*, 2009]. At 10‰ glacial meltwater, the signal-to-noise ratio for neon is still 15:1. The resulting gas ratios are $^{\Delta He}/_{\Delta Ar} = -26.8$, $^{\Delta Ne}/_{\Delta Ar} = -18.7$, $^{\Delta Kr}/_{\Delta Ar} = 4.7$, and $^{\Delta Xe}/_{\Delta Ar} = 7.0$ (Figure 1).

3. Meltwater Mixing in Seawater

While glacial melt and wind-driven bubble exchange, both introduce excess air into the ocean, they yield unique gas concentrations and saturation anomalies. Glacial melt involves a phase change of H_2O concurrent with the addition of air and freshwater to the mixture at a constant ratio. In contrast, wind-driven bubble exchange is the progressive addition of air to the mixture, without the attendant addition of freshwater. We will first explain how meltwater addition affects gas concentration and next how it affects the saturation anomaly.

The unique patterns in gas concentration can be explained as the combination of two effects: (1) The distinct atmospheric partial pressure of each gas and (2) their wide range of solubilities. For example, the solubility of Xe is 17 times greater than Ne while the concentration of Ne in the atmosphere is 209 times greater than Xe. The addition of glacial melt with a fixed amount of trapped air introduces large quantities of a low-solubility gas (e.g., Ne) and smaller quantities of a high-solubility gas (e.g., Xe) relative to saturated seawater. One kilogram of pure glacial meltwater should contain 200.0×10^{-8} cm^3 STP g^{-1} of Ne and 0.99×10^{-8} cm^3 STP g^{-1} of Xe. One kilogram of saturated seawater at $T = 0$, $S = 34$ contains 18.2×10^{-8} cm^3 STP g^{-1} of Ne and 1.45×10^{-8} cm^3 STP g^{-1} of Xe (see Figure S2 in the supporting information). That is, glacial meltwater has significantly more Ne but slightly less Xe than seawater. The change in gas concentration from meltwater addition is depicted as a "solid" line in Figure S1.

In addition to the differences in gas concentration described above, the saturation anomaly is further modified by meltwater addition, which lowers salinity in the seawater admixture, increasing the gas solubility (decreasing the saturation anomaly, Figure S2). Moreover, the latent heat consumed by ice melting causes a substantial reduction in temperature, which in turn decreases the gas saturation anomaly (Figure S2). For example, pure glacial meltwater would have a potential temperature equal to $\theta^* = \theta_f - \frac{L_f}{c_p} - \frac{c_i}{c_w}(\theta_f - \theta_i)$ where $\theta_f, \theta_i, L_f, c_i,$ and c_p are the freeze-point temperature, far-field ice temperature, latent heat of melting, and heat capacities of ice and water, respectively [*Jenkins*, 1999]. Under an ice shelf, salinity and pressure lower the freezing point [*Holland and Jenkins*, 1999]. If θ_i is −20°C and the freezing point temperature is −2.6°C, then the temperature of pure meltwater is ~ −95°C. This was the observational insight of *Gade* [1979] who noted that subsurface melt (under icebergs and ice shelves) produced a linear relationship for $\frac{dT}{dS}$. For example, the *T-S* slope for Muir inlet is 2.56°C ppt^{-1} [*Gade*, 1979]. If this is extrapolated from ambient fjord water ($S = 31$, $T = 3.3$°C) to $S = 0$, the mixing line predicts $\theta^* = -76$°C, not quite as low as the prediction of $\theta^* = -95$°C but of similar magnitude. Like all water types, the pure end-member is an artificial construct [*Poole and Tomczak*, 1999], but it serves to diagnose and model the individual components that we observe in the seawater mixture.

4. Air Injection Versus Glacial Meltwater

When the gas content of glacial ice and the mixing of cold, fresh glacial meltwater are both accounted for, it is apparent that the addition of glacial meltwater is distinguishable from air bubble effects, especially when the heavy NGs are used. This distinction can be observed in Figure 1 by viewing the saturation anomaly patterns for glacial melt as compared to wind-driven air bubble injection and partial bubble exchange. The cooling and freshening effect on solubility causes the three heaviest NGs to become undersaturated with addition of glacial meltwater, and this tendency is opposite to Ne and He, which become progressively oversaturated.

To illustrate the noble gas saturation anomaly ratios of a region characterized by the presence of glacial meltwater, we have included in Figure 1 results from a hydrographic section near the boundary between the Weddell Sea and the Antarctic Circumpolar Current (ACC), during the Antarctic Deep Water Rates of Export (ANDREX) project [*Jullion et al.*, 2010; *Meredith et al.*, 2011]. The full suite of noble gas, helium isotope, and hydrographic results are being reported as part of a larger study that is currently in preparation. The ANDREX section extends east from the tip of the Antarctic Peninsula along 60°S until reaching the 35°E meridian. Figure 1 also includes a line indicating the trend in saturation anomaly that results from seasonal heating and cooling at the ocean surface. In general, excess Ne and He, and a deficit in Ar, Kr, and Xe characterize the ANDREX section. The scatter of the ANDREX points fall between the lines that represent glacial meltwater addition and seasonal cooling from a temperature of −0.15°C, which was the average surface water temperature during ANDREX. This pattern in the sample scatter indicates that the observed excess gas saturation is most simply explained by the seasonal temperature cycle of the surface ocean and the variable addition of glacial meltwater. The lack of glacial meltwater signal in the surface samples is consistent with the evidence that meltwater in the Weddell Sea is formed from cold "high-salinity shelf water" and therefore is too dense to be found near the ocean surface [*Schlosser et al.*, 1990]. Most of the Weddell Sea is covered by sea ice year round. In 2010 the annual average sea ice concentration south of the ANDREX section was 68%, based on the National Snow and Ice Data Center 25 km bootstrap data product [*Comiso*, 2007]. Anecdotally, it is thought that wave breaking and bubble-mediated gas exchanges are suppressed in the seasonal sea ice zone and this appears to be borne out in the ANDREX samples. There are five surface samples in Figure 1 with ΔAr > 0% and excess saturation in Kr and Xe as well. These samples were collected east of the prime meridian, close to the ACC where the water is warmer, free of sea ice for most of the year, and the winds are stronger. These samples cluster much more closely to the air injection line, which is consistent with what is known about the wind and ice conditions at this latitude. ΔHe is elevated with respect to ΔAr and the other anomalies (Figure 1) causing the saturation anomalies to fall above the trend driven by seasonal heating and cooling. This additional deviation in the saturation anomaly is likely the influence of primordial helium introduced through hydrothermal vents, which are often found in water masses that pass over mid-ocean ridges [*Well et al.*, 1999].

The subsurface noble gas samples (dots in Figure 1) were collected more than 500 km from the Larsen C ice shelf and more than 1500 km from the Filchner-Ronne ice shelf, yet the signal provides a clear indication of glacial meltwater in the deep water that is exported from the Weddell Sea, and this is consistent with prior meltwater studies in the Weddell Sea [*Schlosser et al.*, 1990; *Weppernig et al.*, 1996; *Rodehacke et al.*, 2006].
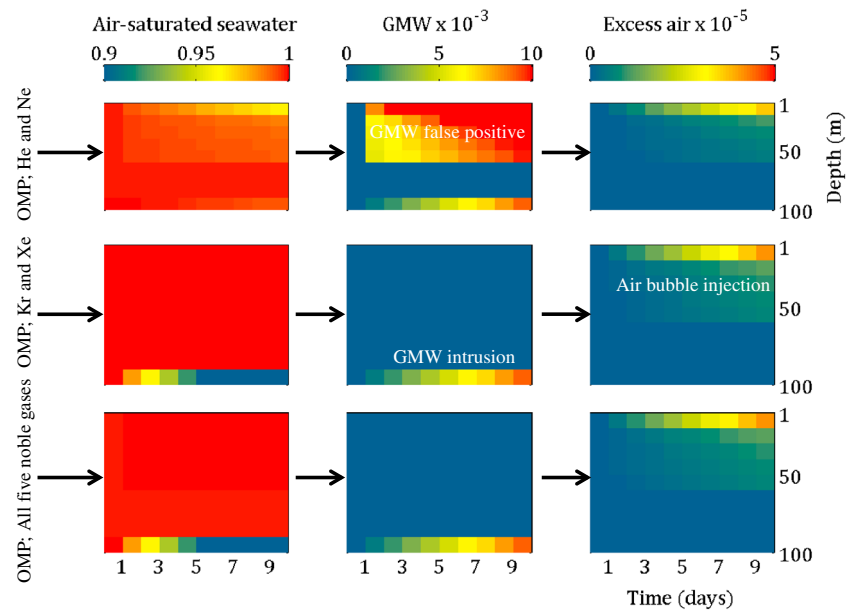
Figure 2. Air bubble injection and glacial meltwater intrusion, illustrated using OMP to separate the component types in a hypothetical ocean surface layer. Ambient seawater ($T = 0°C$, $S = 34$), glacial meltwater, and air are separated into their respective fractions utilizing (top) He and Ne, (middle) Kr and Xe, and utilizing (bottom) all five noble gases. The figure illustrates the progressive bubble injection of air into a 50 m ocean surface layer simulated using the equation for air bubble injection from *Stanley et al.* [2006] with a steady 10 m s^{-1} wind speed over 10 days. At 100 m, 10‰ glacial meltwater is progressively added over the same period.

5. OMP Separation for Glacial Melt and Wind-Driven Air Bubble Injection in a Hypothetical Ocean Surface Layer

In this section, we attempt to demonstrate how the five NGs might be used to quantitatively separate air bubble effects from glacial meltwater using an OMP calculation [*Poole and Tomczak*, 1999]. A hypothetical 100 m ocean surface layer with air-saturated seawater of $T = 0°C$ and $S = 34$ psu is initially at solubility equilibrium for all the NGs. Over 10 days, the ocean experiences air bubble entrainment from a constant wind speed of 10 m s^{-1}. Additionally, glacial meltwater is added to the 100 m depth until 10‰ glacial meltwater content is achieved. The resultant noble gas concentrations can be used with the OMP to map the three end-member components: (1) air-saturated seawater, (2) excess air, and (3) glacial meltwater. We solve the OMP 3 times, first using He and Ne, next using Kr and Xe, and finally using all five NGs. In the first two cases we are using two tracers and mass conservation, so the solution is exactly determined. Additional information on the OMP method used here can be found in section S2 in the supporting information.

When He and Ne alone are used in the mulitparameter solution, a "false positive" of glacial meltwater appears (Figure 2); up to 38.8‰ of glacial meltwater is found in the upper 50 m, where no meltwater was added. This false positive results because air injection and glacial meltwater have similar effects on He and Ne (Figures 1 and S2), so the two inputs are easily confused. When Kr and Xe alone are used in the mulitparameter solution, there is no false positive for glacial meltwater, and the same occurs when all five NGs are used (Figure 2). In all three calculations, the model-data misfit is less than 0.16%; the typical threshold for rejecting the OMP fit to the data is $> 5\%$. While the total model-data misfit is low, the false positive for glacial meltwater also causes the excess air to be underestimated when He and Ne alone are used. The total air bubble content introduced to the hypothetical ocean was 30.08 mol m^{-2} by day 10. The solution with He and Ne alone reproduces 26.17 mol m^{-2}, with Kr and Xe alone reproduces 29.52 mol m^{-2}, and all five NGs together reproduces 30.26 mol m^{-2}, so the fit quality is best when all five NGs are used and the solution is overdetermined. All three solutions reproduce the glacial meltwater content at 100 m exactly.

Simulating excess air as a pure end-member probably has limited applicability, because determining its end-member composition in terms of other important water mass tracers such as, e.g., temperature, salinity, and $\delta^{18}O$ would be difficult. When using all five NGs with real data, it will be necessary to isolate a water type that

is known to have experienced air bubble injection but minimal meltwater addition. In the case where this is not possible, an iterative solution or extended OMP solution [*Karstensen and Tomczak*, 1998] may be possible.

6. Summary

The heavy noble gases exhibit unique saturation anomalies when glacial meltwater is mixed with ambient seawater. These anomalies can be explained by the relatively fixed gas content that is thought to exist in glacial ice and by the solubility effect of mixing cold, fresh meltwater with seawater. The saturation anomaly ratios for light and heavy noble gases are distinct from each other and from other physical processes that modify the gas saturation state, namely, seasonal heating/cooling and air injection. The unique saturation signature of each of the five noble gases makes them an invaluable suite of tracers for optimal estimation of meltwater content.

References

Alley, R. B., P. U. Clark, P. Huybrechts, and I. Joughin (2005), Ice-sheet and sea-level changes, *Science*, *310*, 456–460.

Comiso, J. C. (2007), *Bootstrap sea ice concentrations from Nimbus-7 SMMR and DMSP SSM/I*, National Snow and Ice Data Center, Boulder, Colo. [Available at http://nsidc.org/data/nsidc-0079.]

Craig, H., Y. Horibe, and T. Sowers (1988), Gravitational separation of gases and isotopes in polar ice caps, *Science*, *242*(4886), 1675–1678.

Emerson, S., T. Ito, and R. C. Hamme (2012), Argon supersaturation indicates low decadal-scale vertical mixing in the ocean thermocline, *Geophys. Res. Lett.*, *39*, L18610, doi:10.1029/2012GL053054.

Gade, H. (1979), Melting of ice in sea water: A primitive model with application to the Antarctic ice shelf and icebergs, *J. Phys. Oceanogr.*, *9*, 189–198.

Goddijn-Murphy, L., D. K. Woolf, and C. Marandino (2012), Space-based retrievals of air-sea gas transfer velocities using altimeters: Calibration for dimethyl sulfide, *J. Geophys. Res.*, *117*, C08028, doi:10.1029/2011JC007535.

Hamme, R. C., and S. R. Emerson (2006), Constraining bubble dynamics and mixing with dissolved gases: Implications for productivity measurements by oxygen mass balance, *J. Mar. Res.*, *64*, 73–95.

Hamme, R. C., and J. P. Severinghaus (2007), Trace gas disequilibria during deep-water formation, *Deep Sea Res., Part I*, *54*(6), 939–950.

Hellmer, H. H., O. Huhn, D. Gomis, and R. Timmermann (2011), On the freshening of the northwestern Weddell Sea continental shelf, *Ocean Sci.*, *7*(3), 305–316.

Hohmann, R., P. Schlosser, S. Jacobs, A. Ludin, and R. Weppernig (2002), Excess helium and neon in the southeast Pacific: Tracers for glacial meltwater, *J. Geophys. Res.*, *107*(C11), 3198, doi:10.1029/2000JC000378.

Holland, D. M., and A. Jenkins (1999), Modeling thermodynamic ice-ocean interactions at the base of an ice shelf, *J. Phys. Oceanogr.*, *29*(8), 1787–1800.

Ito, T., R. C. Hamme, and S. Emerson (2011), Temporal and spatial variability of noble gas tracers in the North Pacific, *J. Geophys. Res.*, *116*, C08039, doi:10.1029/2010JC006828.

Jacobs, S. S., H. H. Hellmer, C. S. M. Doake, A. Jenkins, and R. M. Frolich (1992), Melting of ice shelves and the mass balance of Antarctica, *J. Glaciol.*, *38*(130), 375–387.

Jacobs, S. S., C. F. Giulivi, and P. A. Mele (2002), Freshening of the Ross Sea during the late 20th century, *Science*, *297*(5580), 386–389.

Jenkins, A. (1999), The impact of melting ice on ocean waters, *J. Phys. Oceanogr.*, *29*(9), 2370–2381.

Jullion, L., S. C. Jones, A. C. Naveira Garabato, and M. P. Meredith (2010), Wind-controlled export of Antarctic Bottom Water from the Weddell Sea, *Geophys. Res. Lett.*, *37*, L09609, doi:10.1029/2010GL042822.

Karstensen, J., and M. Tomczak (1998), Age determination of mixed water masses using CFC and oxygen data, *J. Geophys. Res.*, *103*(C9), 18,599–18,609.

Keeling, R. F. (1993), On the role of large bubbles in air-sea gas exchange and supersaturation in the ocean, *J. Mar. Res.*, *51*, 237–271.

Loose, B., P. Schlosser, W. M. Smethie, and S. Jacobs (2009), An optimized estimate of glacial melt from the Ross Ice Shelf using noble gases, stable isotopes, and CFC transient tracers, *J. Geophys. Res.*, *114*, L05603, doi:10.1029/2008JC005048.

Martinierie, P., D. Raynaud, D. M. Etheridge, J.-M. Barnol, and D. Mazaudier (1992), Physical and climatic parameters which influence the air content in polar ice, *Earth Planet. Sci. Lett.*, *112*, 1–13.

Meredith, M. P., A. L. Gordon, A. C. Naveira Garabato, E. P. Abrahamsen, B. A. Huber, L. Jullion, and H. J. Venables (2011), Synchronous intensification and warming of Antarctic Bottom Water outflow from the Weddell Gyre, *Geophys. Res. Lett.*, *38*, L03603, doi:10.1029/2010GL046265.

Nicholson, D., S. Emerson, N. Caillon, J. Jouzel, and R. C. Hamme (2010), Constraining ventilation during deepwater formation using deep ocean measurements of the dissolved gas ratios 40Ar/36Ar, N2/Ar, and Kr/Ar, *J. Geophys. Res.*, *115*, C11015, doi:10.1029/2010JC006152.

Orsi, A. H., G. C. Johnson, and J. L. Bullister (1999), Circulation, mixing and production of Antarctic Bottom Water, *Prog. Oceanogr.*, *43*, 55–109.

Poole, R., and M. Tomczak (1999), Optimum Multiparameter analysis of the water mass structure in the Atlantic Ocean thermocline, *Deep Sea Res. Part A*, *46*, 1895–1921.

Rignot, E., and S. S. Jacobs (2002), Rapid bottom melting near Antarctic ice sheet grounding lines, *Science*, *296*, 2020–2023.

Rodehacke, C. B., O. Huhn, V. Hellmer, and A. Beckmann (2006), Ocean/ice shelf interaction in the southern Weddell Sea: Results of a regional numerical helium/neon simulation, *Ocean Dyn.*, doi:10.1007/s10236-006-0073-2.

Schlosser, P. (1986), Helium: A new tracer in Antarctic Oceanography, *Nature*, *321*, 233–235.

Schlosser, P., W. Roether, and G. Rohardt (1987), Helium-3 balance of the upper layers of the northwestern Weddell sea, *Deep Sea Res. Part A*, *34*(3), 365–377.

Schlosser, P., R. Bayer, A. Foldvik, T. Gammelsröd, G. Rohardt, and O. K. Münnich (1990), Oxygen 18 and Helium as tracers of ice shelf water and water/ice interaction in the Weddell Sea, *J. Geophys. Res.*, *95*(C3), 3253–3263.

Severinghaus, J. P., and M. O. Battle (2006), Fractionation of gases in polar ice during bubble close-off: New constraints from firn air Ne, Kr and Xe observations, *Earth Planet. Sci. Lett.*, *244*(1–2), 474–500.

LOOSE AND JENKINS 2840

Stanley, R., W. J. Jenkins, and S. C. Doney (2006), Quantifying seasonal air-sea gas exchange processes using noble gas time-series: A design experiment, *J. Mar. Res.*, *64*, 267–295.

Stanley, R. H. R., G. Baschek, D. E. I. Lott, and W. J. Jenkins (2009), A method for measuring noble gases and their isotopic ratios using programmed multistage cryogenic trapping and a combination of quadrupole and magnetic sector mass spectrometers, *Geochem. Geophys. Geosyst.*, *10*, Q05008, doi:10.1029/2009GC002429.

Well, R., W. Roether, and D. P. Stevens (1999), An additional deep-water mass in Drake Passage as revealed by ^{3}He data, *Deep Sea Res., Part I*, *50*(9), 1079–1098.

Weppernig, R., P. Schlosser, S. Khatiwala, and R. G. Fairbanks (1996), Isotope data from Ice Station Weddell: Implications for deep water formation in the Weddell Sea, *J. Geophys. Res.*, *101*(C10), 25,723–25,739.